IEEE Access
Multidisciplinary | Rapid Review | Open Access Journal

IEEE ENGINEERING IN MEDICINE AND BIOLOGY SOCIETY SECTION

Received April 20, 2021, accepted May 11, 2021, date of publication May 24, 2021, date of current version June 8, 2021.

Digital Object Identifier 10.1109/ACCESS.2021.3083088

Triple Coaxial-Half-Slot Antenna Scheme With Deep Learning-Based Temperature Prediction for Hepatic Microwave Ablation: Finite Element Analysis and In Vitro Experiment

PATTARAPONG PHASUKKIT, (Member, IEEE), AND TEERASAK WONGKETSADA
School of Engineering, King Mongkut's Institute of Technology Ladkrabang, Bangkok 10520, Thailand

Corresponding author: Pattarapong Phasukkit (pattarapong.ph@kmitl.ac.th)

This work was supported in part by the KMITL Research and Innovation Services (KRIS) of the King Mongkut's Institute of Technology Ladkrabang.

ABSTRACT This research proposes a triple-antenna scheme of three coaxial half slot antennas (CHSA) for minimally invasive hepatic microwave ablation (MWA). In the MWA treatment, the antennas were positioned around the cancer tissue in equilateral triangle formation, with the half-slot side of the antennas directed at the triangle center to concentrate the microwave energy. Finite element (FE) simulations and in vitro experiments with swine liver were carried out to determine the temperatures and coagulation zone under different distances between the three antennas: 10, 20, and 30 mm. Besides, a regression-based deep learning algorithm was utilized to predict temperatures at the midpoint of the triple-CHSA arrangement without inserting a temperature sensor into the targeted tissue. The algorithm relied on temperatures at a site adjacent to the targeted cancer tissue to predict the midpoint temperatures. The triple-CHSA scheme could achieve a large coagulation zone with temperatures of 60 °C or higher. The FE simulation results showed that the largest coagulation volumes achieved were 18.425, 29.312, and 63.507 cm^3 for the between-antenna distances of 10, 20, and 30 mm, respectively. The largest coagulation volumes of in vitro experiments were 18.437, 29.317, and 63.504 cm^3 for the corresponding between-antenna distances. The prediction accuracy of the deep learning algorithm were 99.98 % for mean square error, 98.75 % for mean absolute error, and 99.22 % for mean absolute percentage error. The novelty of the research lies in the use of CHSA surrounding the cancer tissue in equilateral triangle formation for hepatic MWA, as opposed to the conventional hepatic MWA procedure which requires inserting antennas into the targeted tissue. Another research novelty is the use of regression-based deep learning algorithm to predict the temperature of liver tissue at the midpoint of the triple-CHSA arrangement.

INDEX TERMS Triple antenna, microwave (MA) ablation, Coaxial-half-slot antenna, temperature prediction, finite element (FE) analysis, in vitro experiment, directional.

I. INTRODUCTION

Consumption of undercooked meat and excessive alcohol use contribute to the prevalence of hepatic cancer in several Southeast Asian countries, and the situation has worsened with the passing years despite efforts to increase awareness. The current treatment options for liver cancer are thermal therapy and thermotherapy combined with chemotherapy [1]. The thermal therapy commonly used to treat hepatic cancer include radiofrequency ablation, cryoablation, and microwave ablation.

Radiofrequency Ablation (RFA) is a medical procedure whereby the cancer tissue (i.e., targeted area) is ablated by the heat generated from medium frequency alternating current (350 – 500 KHz). Nevertheless, the RFA procedure is less effective if the targeted area is adjacent to a blood vessel with relatively high flow. The high-flow blood vessel renders the ablation temperatures too low to completely destroy the cancer cells. In addition, high impedance between the electrode and ground plate as a result of an increase in tissue

The associate editor coordinating the review of this manuscript and approving it for publication was Kin Fong Lei.

temperature during the RFA procedure also reduces the treatment effectiveness [2]–[4].

Cryoablation (CA) is a medical procedure that uses extreme cold from compressed argon gas to destroy cancer tissue. In cryoablation, cryoprobes (i.e., hollow needles) are positioned adjacent to the targeted area, and cooled, thermally conductive, fluids are circulated through hollow needles to destroy the diseased tissue. However, the CA destruction zone is confined to small areas surrounding the hollow needles, and the procedure can cause damage to the phrenic nerve [5].

To overcome the drawbacks of RFA and CA, microwave (MW) frequency in ISM band (industrial, scientific and medical) of 915 MHz and 2450 MHz (the center frequency) have been adopted to ablate and destroy the diseased tissue. Microwave ablation (MWA) is a treatment option for cancer patients with unresectable hepatic malignancies [6], [7]. In [7], MWA was comparatively carried out with tissues using three MW center frequencies (915 MHz and 2450 MHz). The ablation temperatures of 60 °C or higher lead to near-instantaneous cell death [8].

The advantages of MWA include short MW-to-thermal conversion time, minimal side-effect, high treatment effectiveness, and very lower cancer recurrence of only 2 % [9]. Therefore, single- and multiple-antenna schemes have been proposed for MWA treatment of diseased tissue. The main advantage of single-antenna MWA schemes is the ability to specify the destruction pattern. However, the single-antenna schemes fail to achieve large destruction areas. As a result, multi-antenna MWA schemes of various configurations have been developed. The multi-antenna schemes for MWA treatment could achieve specific destruction patterns and large areas of cancer tissue destruction.

For the single-antenna MWA schemes, a single triaxial antenna MWA scheme was proposed and experiments carried out using ex vivo bovine liver [10]. In [11], an adjustable sliding chock MWA antenna could achieve the destruction size of 1 – 2 cm in radius with spherical shape. Meanwhile, a MWA coaxial single-slot antenna was designed and experiments carried out to treat bone tumors [12]. In [13], a cap-choke catheter antenna was proposed for MWA treatment, and a floating sleeve MWA antenna was developed for treating hepatic cancer [14]. In addition, a dual-slot coaxial single-antenna scheme was developed to treat cancer tissue using microwave [15]. In [16], a multi-slot coaxial MW single-antenna scheme was proposed to ablate liver tumors.

However, the first generation of single-antenna MWA schemes lacks the directional capability (i.e., the inability to manipulate the direction of MW energy), giving rise to symmetrical coagulation shape. The coagulation symmetry renders the first-generation single-antenna MWA schemes unsuitable for ablation in zones adjacent to critical areas. As a result, a directional single-sided open interstitial single-antenna scheme was proposed for MWA, and the MW direction of the proposed antenna scheme is manipulatable [17], [18]

Moreover, to achieve larger cancer tissue destruction or coagulation zone, multi-antenna schemes of varying configurations have been proposed for MWA, and the multi-antenna schemes could achieve larger coagulation zone with minimal invasiveness, in comparison with the single-antenna scheme [19]. In [20], the single- and multiple-antenna (dual- and triple-antenna) MWA schemes were compared in terms of the coagulation zone. Besides, the configurations of the triple-antenna MWA scheme were varied and experimental results showed that the triangular arrangement achieved the largest coagulation zone.

In [21], the effect of phase shift on a triple-antenna scheme for hepatic MWA was investigated using 3D finite element simulation. The results showed that phase shift between antennas from 90°, 180° to 270° affected the coagulation volume, and the triple-antenna scheme could achieve asymmetrical destruction patterns.

In [22], a triple-antenna scheme for hepatic MWA was proposed and in vitro experiments carried out. The results showed that the triple-antenna scheme could achieve larger destruction zone, in comparison with the single-antenna MWA scheme. In [23], array multi-antenna schemes were proposed for MWA and experiments carried out under in vivo and ex vivo conditions. Reference [24], [25] proposed double-slot triple-antenna schemes in triangular array for MWA and experiments carried out under in vivo conditions. The results showed that the double-slot triple-antenna schemes achieved larger ablation zones than the single-antenna scheme.

In the conventional MWA procedures, the antennas need to be inserted into the center of the targeted tissue to ablate. In the event that the ablation target is adjacent to critical areas, great care must be exercised to prevent thermal damage to non-targeted critical areas while achieving complete coverage of the targeted tissue. Fluid installation between the targeted and non-targeted sites susceptible to thermal damage is thus adopted to reduce thermal damage to the non-targeted tissues [26]. Alternatively, directional-radiation MW antennas could be deployed to ablate the targeted site adjacent to critical structures without fluid installation. Besides, in the conventional MWA, a temperature probe needs to be inserted into the targeted site to monitor the temperatures of the targeted tissue, further injuring the cancer tissue.

Specifically, this research proposes a triple-antenna MWA scheme to treat liver cancer. The proposed scheme consisted of three coaxial half slot antennas (CHSA) surrounding the cancer tissue in equilateral triangle formation. The half-slot side of the three antennas were directed at the midpoint of the triangle to concentrate the MW energy at the center. Finite element simulations and in vitro experiments using freshly slaughtered swine liver were carried out to determine the temperatures and coagulation zone. In addition, a deep learning algorithm was proposed to predict temperatures of the liver tissue at the midpoint of the triple-CHSA arrangement without inserting a temperature sensor into the targeted liver tissue. The algorithm predicts the midpoint temperature based

on temperatures at the site adjacent to the targeted cancer tissue.

II. ANTENNA DESIGN AND FINITE ELEMENT MODELING

In this research, the antenna was of semirigid coaxial cable with a diameter of 3.581 mm (M17/130-RG402 copper jacket, EMC Technology & Florida RF Labs) connected to N-type connector. A half slot of 10 mm in length was cut on the outer conductor for a coaxial half slot (CHS) antenna. The remaining half of the outer conductor (opposite the half slot) functions as the reflector. The center of the half slot was 15 mm from the distal end of the coaxial antenna. The length of CHS antenna excluding the N-type connector was 60 mm, as shown Fig 1. The CHS antenna structure was subsequently simulated using 3D finite element (FE) under two scenarios: single and triple CHS antennas. Table 1 tabulates the dimensions of the CHSA parameters.

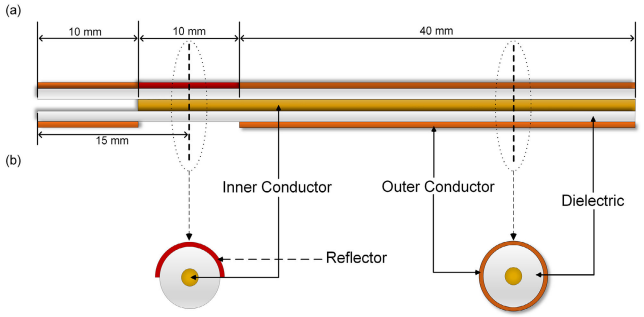

FIGURE 1. The structure of coaxial half slot (CHS) antenna: (a) longitudinal orthogonal view, (b) transverse view of two sections.

TABLE 1. Dimensions of the CHSA parameters.

Parameter	Dimension (mm)
Diameter of inner conductor	0.912
Diameter of dielectric	2.985
Diameter of outer conductor	3.581
Half-slot length	10
Length from one end to midpoint of half slot	15
CHS antenna length excluding N-type connector	60

The design of the triple-CHSA scheme is based on the MWA principle where heat generated by microwave energy is used to destroy hepatic cancer. In MWA, three CHS antennas are positioned surrounding the cancer tissue in equilateral triangle formation, with the half-slot side of the triple CHS antennas directed at the midpoint of the triangle to concentrate the MW energy at the center. The use of triple CHS antennas is to achieve a large coagulation zone with temperatures of 60 °C or higher [8].

Fig. 2 shows the voltage standing wave ratio (VSWR) of the triple CHS antennas (Antennas I, II, and III) over

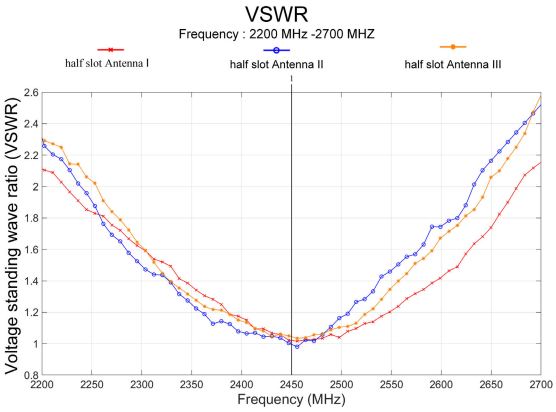

FIGURE 2. Voltage standing wave ratio (VSWR) of CHS antennas (Antennas I, II, III) over 2200 - 2700 MHz.

TABLE 2. Electrical properties of the antenna for application of biomedical (Liver tissue).

Parameter	Values
VSWR at 2.45 GHz	Antenna I = 1.01 Antenna II = 1.08 Antenna III = 1.03
Bandwidth (VSWR <2.0)	Antenna I = 2225-2675 MHz Antenna II = 2237-2680 MHz Antenna III = 2255-2685 MHz
SAR	Single Antenna = 34.46 W/kg Triple Antenna (10 mm) = 627.82 W/kg Triple Antenna (20 mm) = 87.97 W/kg Triple Antenna (30 mm) = 63.12 W/kg
SAR Pattern	Single Antenna / Triple Antenna (10mm) / Triple Antenna (20mm) / Triple Antenna (30mm) 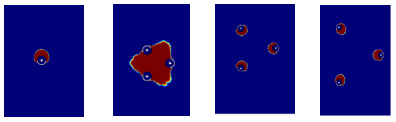

2200 – 2700 MHz, using Bird Site Analyzer (SA-6000 EX, Bird Electronic Corporation, USA). The frequency range (2200 – 2700 MHz) covers the MW frequency in ISM band of 2450 MHz (center frequency). The measurement was carried out by individually inserting the CHS antennas (Antennas I, II, and III) into 10 cm × 10 cm freshly slaughtered swine liver. The resulting VSWR at the center frequency of the three CHS antennas were approximately 1.006 (good impedance matching). The very low VSWR rendered the CHS antennas operationally suitable for hepatic MWA because MW energy can be efficiently delivered into the liver tissue.

Table 2. show electrical properties of the antenna for application of biomedical tissue were added to the table, detailing the VSWR of each antenna at 2450MHz

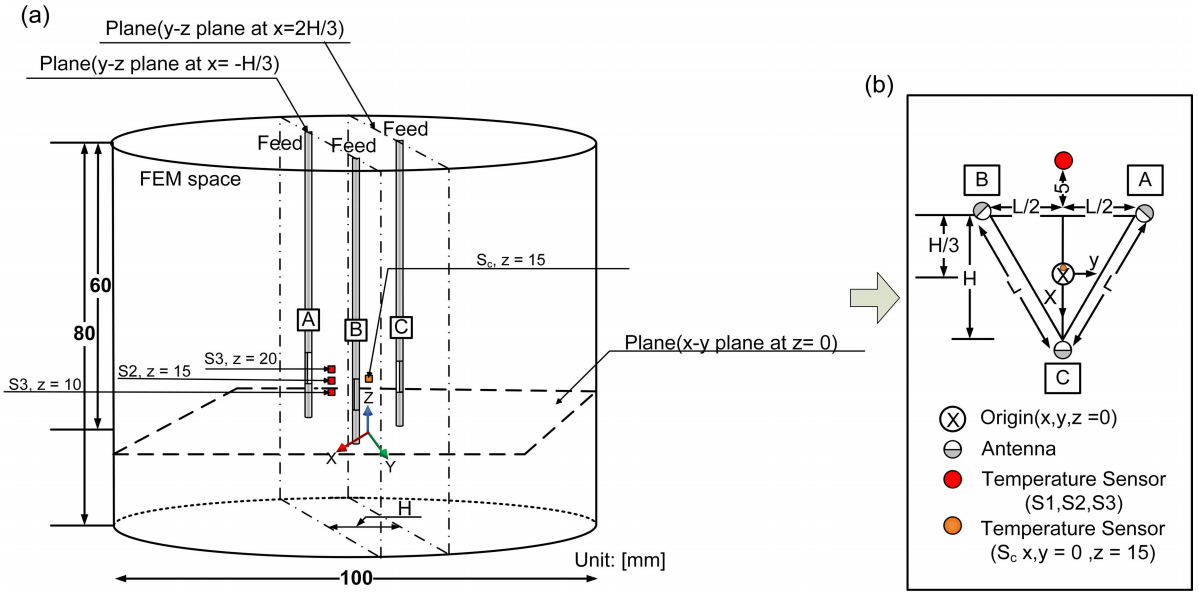

FIGURE 3. The proposed triple-CHSA scheme for hepatic MWA, where I, II, and III denote Antennas I, II, and III; and Sc, S1, S2, and S3 denote the temperature sensor at the midpoint and temperature sensors 1 – 3.

(operation frequency) and the usable bandwidth of each antenna, from antenna I = 2225 - 2675 MHz, antenna II = 2237 - 2680 MHz and antenna III = 2255 - 2685 MHz. The Specific Absorption Rate (SAR) of single antenna = 34.46 W/kg, Triple Antenna (10 mm) = 627.82 W/kg, Triple Antenna (20 mm) = 87.97 W/kg and Triple Antenna (30 mm) = 63.124 W/kg. SAR patterns depend on the spacing of the electromagnetic field that is emitted from each antenna position. A triple antenna with a spacing of 10 mm is the most collect SAR value compared with 20 mm and 30 mm of antenna spacing.

In MWA, the source of heat transfer is electromagnetic wave at the center frequency (2450 MHz) transmitted into tissue. Joule heating arises when an electric current pass through a conductor and is converted into thermal energy. In FE modeling, changes in tissue temperature over time can be mathematically expressed by the bioheat, as shown in (1).

$$\rho C \frac{\partial T}{\partial t} + \nabla (-k \nabla T) = -Q_p + Q_{met} + Q_{ext} \tag{1}$$

where ρ is tissue density (kg/m^3), C is specific of heat (J/kg·K), T is temperature thermal (K), t is time (s), and k is thermal conductivity (W/m)

$$Q_{ext} = \rho \mathrm{SAR} \tag{2}$$

$$SAR = \frac{\sigma}{2\rho} E^2 \tag{3}$$

Therefore

$$Q_{ext} = \frac{\sigma E^2}{2} \tag{4}$$

where SAR is specific absorption rate of tissue, σ is electrical conductivity (S/m), and E = electric field vector (V/m).

TABLE 3. Dielectric properties of liver tissue and CHS antenna at 2450 MHz used in FE modeling [24] [27].

Properties	Value	
Density of liver tissue (ρ_{liver})	1020 kg/m^3	
Specific heat of liver tissue (C_{liver})	20-70 °C	80-100 °C
	3,628 [J/kg·K]	3,858 [J/kg·K]
Thermal conductivity (k_{liver})	20-70 °C	80-100 °C
	0.465 [W/m·K]	0.867 [W/m·K]
Electrical conductivity of liver tissue[1] (σ_{liver})	1.69 [S/m]	
Relative permittivity of liver tissue (ε_{liver})	43.03	
Relative permittivity of dielectric of CHSA (ε_{diel})	2.03	

C_{liver} between 71-79 °C are the average of C_{liver} of 20-70 °C and 80-100 °C, and so k_{liver} between 71-79 °C.
[1]Source: http://niremf.ifac.cnr.it/tissprop/htmlclie/htmlclie.php

Prior to in vitro experiment, the temperature distribution from the triple-CHSA scheme to the liver tissue was characterized, given that the liver temperature distribution is subject to SAR. Table 3 tabulates the dielectric properties of liver tissue and the CHS antenna at 2450 MHz, which were used in the FE modeling (1) – (4).

In FE modeling (1), the energy generated by the metabolic process (Q_{met}) is very negligible and thus ignored. Q_{ext} is generated by microwave energy from antennas, and Q_p is

TABLE 4. FE-simulated coagulation zone and volume using the triple-CHSA scheme under variable between-antenna distances and microwave durations, given 50 W microwave energy.

Distance (mm)	Plane	Width (mm)	Length (mm)	Volume (cm^3)	MW duration (second)
10	XY	15.0	14.5	0.014	60
	ZX	16.8	15.2		
	ZY	18.2	14.8		
20	XY	24.0	21.6	10.807	600
	ZX	16.2	24.0		
	ZY	16.0	22.4		
30	XY	39.0	35.2	42.295	1300
	ZX	20.4	39.0		
	ZY	20.4	35.2		

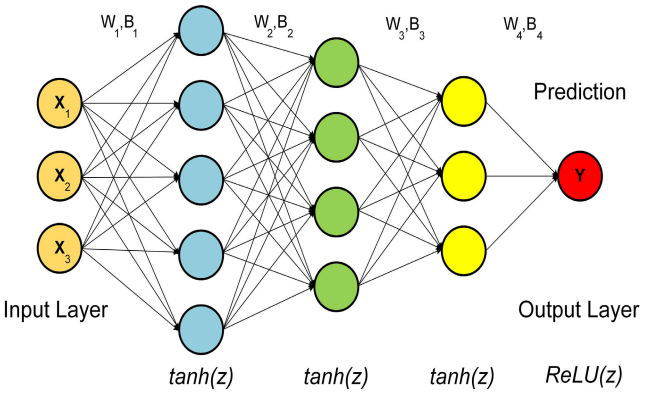

FIGURE 4. The proposed regression-based deep learning algorithm for prediction of midpoint temperature.

energy generated by blood perfusion, which was ignored in this research because the in vitro experiments were carried out using freshly slaughtered swine liver. The Initial Graphics Exchange Specification (IGES) file was used to render 3D computer-aided design (CAD) model (Fig 3), and COMSOL Multiphysics (version 5.5a) was used to simulate the 3D FE model, with the initial and refined mesh in tetrahedral shape, consisting of 1,266,371 elements and the degree of freedom of 8,931,575.

As previously stated, the proposed CHSA scheme was simulated by 3D FE model under two scenarios: single and triple CHS antennas. The single-antenna scenario was carried out in egg white and swine liver using 50 W microwave energy for 100 seconds to characterize the coagulation shape (for egg white) and zone (for swine liver), given the temperature threshold of 60 °C or higher.

Fig 3 illustrates the FE model of the proposed triple-CHSA scheme for hepatic MWA under the triple-antenna scenario. The antennas (Antennas I, II, III) were arranged in equilateral triangular formation parallel to the z-axis. The distance (L) between Antennas I, II, and III in the FE model was varied between 10, 20, and 30 mm, and the insertion depth of the antennas was 60 mm (i.e., the length of CHS antenna without N-type connector).

The overall geometry was of cylindrical shape with 80 mm in height and 100 mm in diameter. The temperature distribution on the x–y plane was characterized at $z = 0$ mm, and that on the y–z plane at $x = 2H/3$ mm and $-H/3$ mm. The temperature measurements were taken by four temperature sensors (S_c, S1, S2, S3). The central temperature sensor (S_c) was located at the midpoint of the triple CHSA arrangement at $x, y = 0$ and $z = 15$ mm. The other temperature sensors (S1, S2, S3) at $z = 10$, $z = 15$, and $z = 20$ mm was located 5 mm from the midpoint between Antennas I and II (Fig 3(b)).

In the FE simulation, the three CHS antennas (Antennas I, II, III) were fed with 50 W microwave power at 2450 MHz from 0 – 2000 seconds. The FE simulation was carried out on a workstation computer with CPU Intel®Xeon®2.70 GHz x 2 and 256 GB of RAM running on 64-bit Microsoft Windows 10 Pro. It required 17 hours 20 minutes 31 seconds to solve the 3D FE model, utilizing 244 GB of RAM.

The FE-simulated temperatures from the four temperature sensors (S_c, S1, S2, S3) were used as training dataset of the proposed regression-based deep learning algorithm (i.e., those of S1, S2, S3 as X_train and Sc as Y_train). Meanwhile, the microwave durations under different between-antenna distances (L; 10, 20, 30 mm) were determined using the FE-simulated coagulation zone and volume, given the midpoint temperature of the triple-antenna arrangement of 60 °C [8], [28]. Furthermore, the FE-simulated microwave durations that achieved the largest coagulation zone and volume, given the midpoint temperature of 100 °C, under three different between-antenna distances (L) were also determined.

III. REGRESSION-BASED DEEP LEARNING ALGORITHM

This research used a regression-based deep learning algorithm to predict temperatures of the liver tissue at the midpoint of the triple-CHSA arrangement (S_c) in place of the central temperature sensor (S_c), where ($\hat{S}_c$) is the deep learning-based predicted midpoint temperature. The deep learning algorithm relied on FE-simulated temperatures from the four temperature sensors (S_c, S1, S2, S3) as the training dataset (X_train and Y_train) to predict the midpoint temperature of the triple-antenna scheme ($\hat{S}_c$) without inserting the central temperature sensor (S_c) into the targeted liver tissue.

Prior to training the deep learning algorithm, the FE-simulated temperatures during MWA (0 – 2000 seconds), given 50 W microwave energy, at S_c, S1, S2, and S3 were collected. To verify the FE model, the FE-simulated temperatures were compared with those of in vitro experiments using swine liver. The in vitro temperature measurements at S_c, S1, S2, and S3 were taken by using a temperature data logger (thermocouple type K; MIDI logger GL840-M). The FE-simulated temperatures (X_train and Y_train) were used to train the regression-based deep learning algorithm, while those of in vitro experiments (X_test and Y_test) were for testing the deep learning algorithm.

Fig 4 illustrates the regression-based deep learning algorithm for prediction the midpoint temperature of the

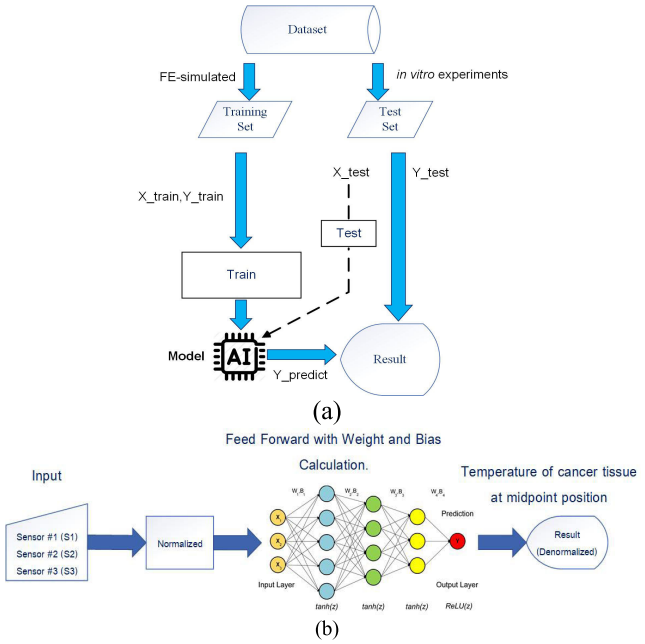

FIGURE 5. (a) Experiment design of regression-based deep learning algorithm for prediction. The datasets are divided into two groups with training and testing groups. (b) The result of the model can then be used to predict a new midpoint temperature in cancer tissue.

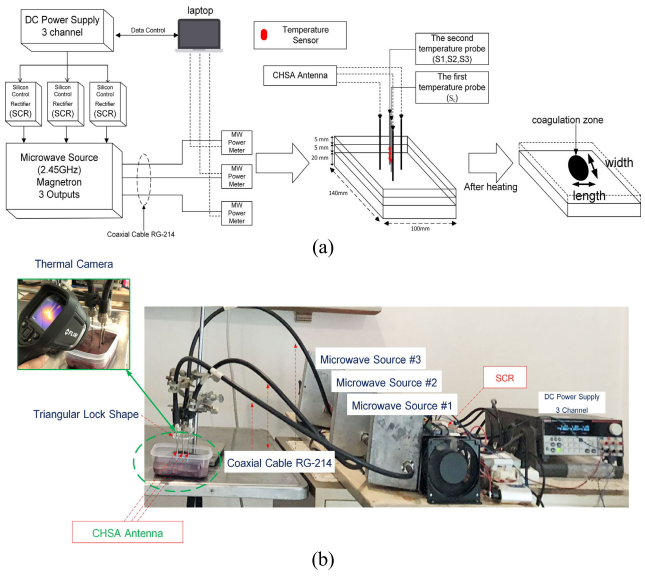

FIGURE 6. (a) Schematic of *in vitro* experimental setup for hepatic MWA. (b) Experiment setup for hepatic microwave ablation and measuring the temperature with the thermal camera.

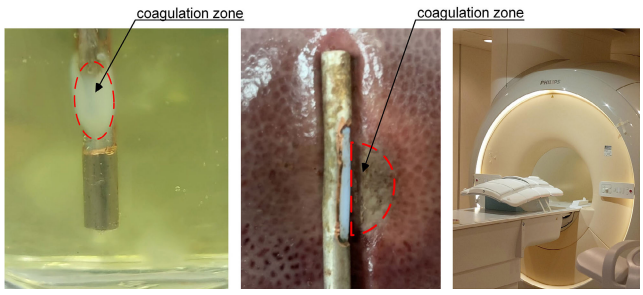

FIGURE 7. *In vitro* experiments: (a) in egg white using single CHS antenna, (b) in swine liver using single CHS antenna, (C) magnetic resonance imaging scan.

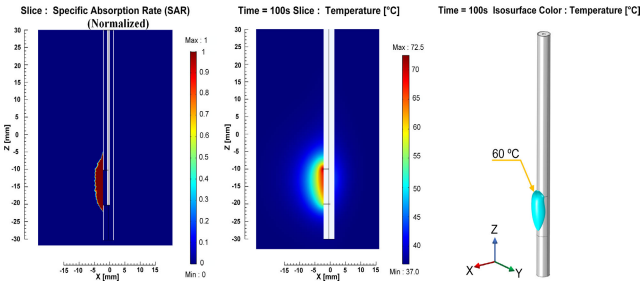

FIGURE 8. FE simulation results using single CHS antenna given 50 W microwave energy for 100 seconds: (a) specific absorption rate in xz plane, (b) temperature distribution in xz plane, (c) 3D coagulation zone with 60 °C or higher.

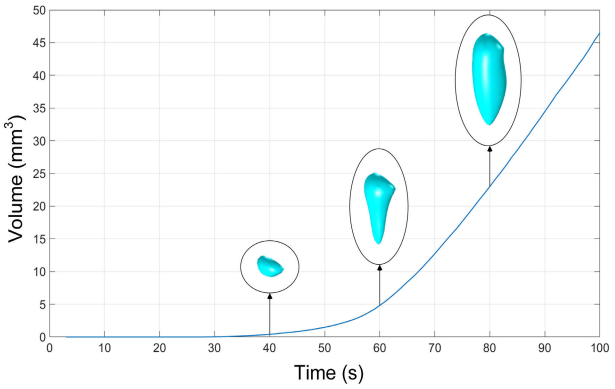

FIGURE 9. FE simulated coagulation volume using single CHS antenna given 50 W microwave energy and 0 – 100 seconds of operating time.

triple-CHSA scheme. The proposed deep learning algorithmic model consisted of one input layer, three hidden layers, and one output layer. The input layer consisted of X_1, X_2, and X_3, where X_1, X_2, and X_3 represent the temperature measurements of the FE model at S1, S2, and S3, respectively. X_1, X_2, and X_3 each contained 2,000 data points (corresponding to 0 – 2000 seconds). The first, second, and third hidden layers had 5, 4, and 3 nodes. Hyperbolic tangent function (tanh(z)) was used as the activation function between hidden layers to transform linear to nonlinear function. The initial weight (W) and bias (B) (W_1, B_1, W_2, B_2, W_3, B_3, W_4, B_4) were random. The output layer (Y) is predicted midpoint temperatures ($\hat{S}_c$). The rectified linear activation function ($ReLU(z)$) was used for positive output values.

The training dataset comprised X_train (normalized input dataset) and Y_train (normalized output dataset). The testing dataset consisted of X_test (normalized input dataset) and Y_test (normalized output dataset). The initial weight (W) and bias (B) in the hidden layers (W_1, B_1, W_2, B_2, W_3, B_3, W_4, B_4) were random, and the learning rate (α) and epoch were 0.01 and 5000. In training the algorithm, W and B were refined by using gradient descent iterative

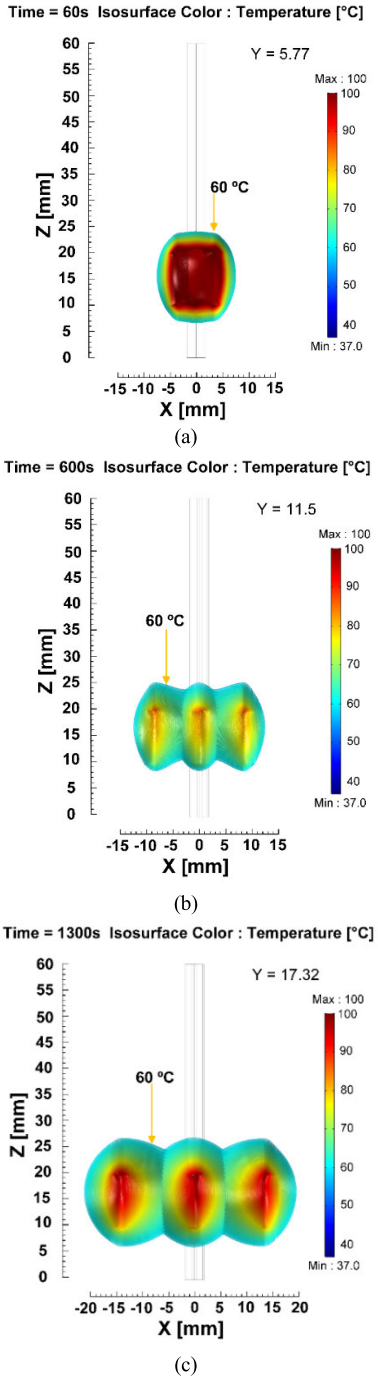

FIGURE 10. FE-simulated coagulation zone using the triple-CHSA scheme in z-x plane, given 50 W microwave energy, for the distance between antennas of: (a) 10 mm given y = 5.77, (b) 20 mm given y = 11.5, (c) 30 mm given y = 17.32.

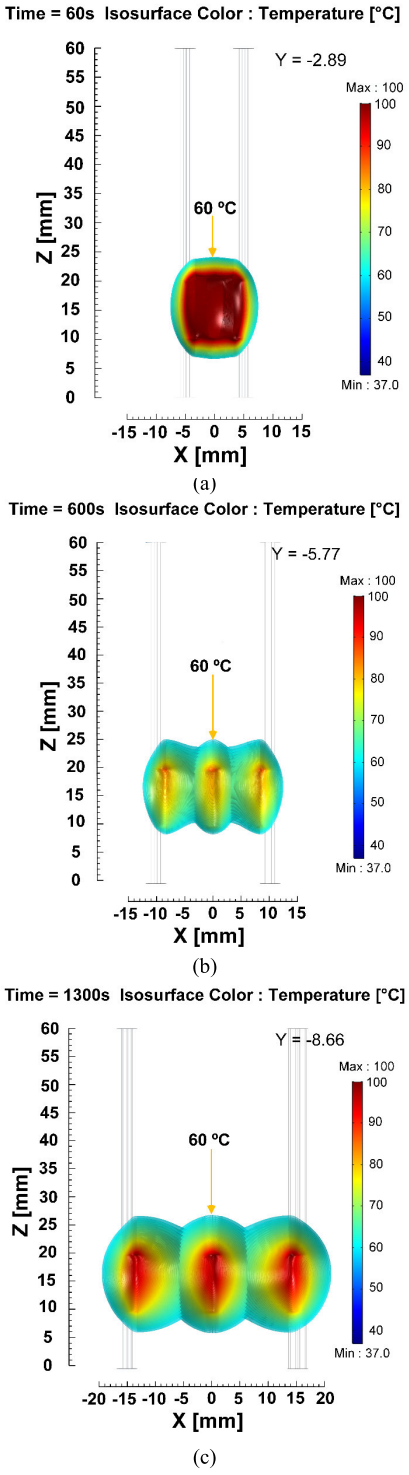

FIGURE 11. FE-simulated coagulation zone using the triple-CHSA scheme in z-x plane, given 50 W microwave energy, for the distance between antennas of: (a) 10 mm given y = −2.89, (b) 20 mm given y = −5.77, (c) 30 mm given y = −8.66.

optimization algorithm. The iteration was terminated once divergence between the mean square errors of the training and testing datasets occurred.

Prior to the training and testing, the training and testing datasets (input and output datasets) were normalized using standardization, as shown in (5)

$$Standardization = \frac{Dataset - Mean\ of\ Dataset}{SD} \quad (5)$$

where *Dataset* is input and output datasets (i.e., X_train, Y_train, X_test, Y_test), *Mean of Dataset* is the mean value of input and output datasets, and *SD* is standard deviation.

In feedforward, hyperbolic tangent function (*tanh(z)*) was the activation function between hidden layers, as shown in (6)

where $tanh(z) = [-1,1]$. The activation function $ReLU(z)$ was used in the output layer, as shown in (7), where z is the linear combination (8). The output of the regression-based deep learning algorithm was the predicted normalized temperature of the liver tissue at the midpoint of the triple-CHSA arrangement ($\hat{S}_c$ or $\hat{y}_n$).

$$tanh\,(z) = \frac{\left(e^{z} - e^{-z}\right)}{\left(e^{z} + e^{-z}\right)} \tag{6}$$

$$ReLU(z) = \begin{cases} 0, & z < 0 \\ z, & z \geq 0 \end{cases} \tag{7}$$

$$Z = \begin{bmatrix} z_1 \\ z_2 \\ \vdots \\ z_N \end{bmatrix} = \begin{bmatrix} x_1^1 w_1 & x_1^2 w_2 & \dots & x_1^D w_D \\ x_2^1 w_1 & x_2^2 w_2 & \dots & x_2^D w_D \\ \vdots & \vdots & \vdots & \vdots \\ x_N^1 w_1 & x_N^2 w_2 & \dots & x_N^D w_D \end{bmatrix} + \begin{bmatrix} B_1 & B_2 & \dots & B_D \end{bmatrix} \tag{8}$$

In back propagation, the Mean Square Error (MSE) between the normalized training output dataset (Y_train; y_n) and predicted normalized output ($\hat{y}_n$) was first calculated ((9)), and then gradient descent iterative optimization algorithm was applied to fine-tune W and B by using (10) and the chain rule derivative.

$$MSE = \frac{1}{n}\sum_{i=1}^{n}\left(y_n - \hat{y}_n\right)^2 \tag{9}$$

$$\frac{\partial MSE}{\partial W_i} \text{ and } \frac{\partial MSE}{\partial B_i} \tag{10}$$

where i = 1, 2, 3, 4 corresponding to $W_1, B_1, W_2, B_2, W_3, B_3, W_4, B_4$; and the derivative of $tanh(z)$ activation function for hidden layers is expressed in (11).

$$\frac{\partial[tanh\,(Az)]}{\partial z} = 1 - \tanh z^2 \tag{11}$$

The prediction performance of the proposed regression-based deep learning algorithm was assessed by Mean Square Error (MSE; (9)), mean absolute error (MAE; (12)), and mean absolute percentage error (MAPE; (13)).

$$MAE = \frac{1}{n}\sum_{i=1}^{n}\left|y_n - \hat{y}_n\right| \tag{12}$$

$$MAPE = \frac{1}{n}\sum_{i=1}^{n}\frac{\left|y_n - \hat{y}_n\right|}{|y_n|} \tag{13}$$

where y_n is the normalized testing output dataset (Y_test), $\hat{y}_n$ is predicted normalized output (Y_predict), and n is the number of datasets.

Fig. 5. (a) shown the design of the regression-based deep learning algorithm model process. After the weight and bias (W_1, B_1, W_2, B_2, W_3, B_3, W_4, B_4) values are optimized in the developing process. Fig. 5. (b) start with normalized input from three sensors (S1, S2, and S3). In the initial step, the temperature values of three sensors are normalized which the normalized data X_1, X_2, and X_3 are feed to deep learning algorithm model. The output (Y) was calculated by the values of W_1, B_1, W_2, B_2, W_3, B_3, W_4, B_4 with were applied in the feedforward process. The result is that actual denormalized temperature at the midpoint of the cancer tissue.

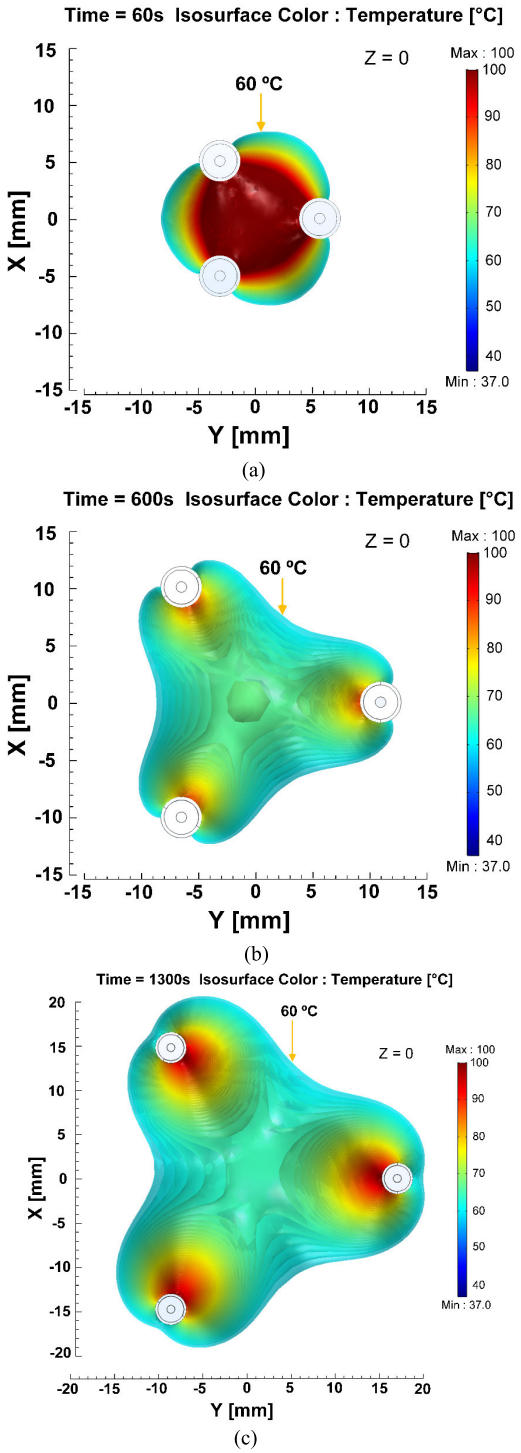

FIGURE 12. FE-simulated coagulation zone using the triple-CHSA scheme in x-y plane, given 50 W microwave energy and z = 0, for the distance between antennas of: (a) 10 mm, (b) 20 mm, (c) 30 mm.

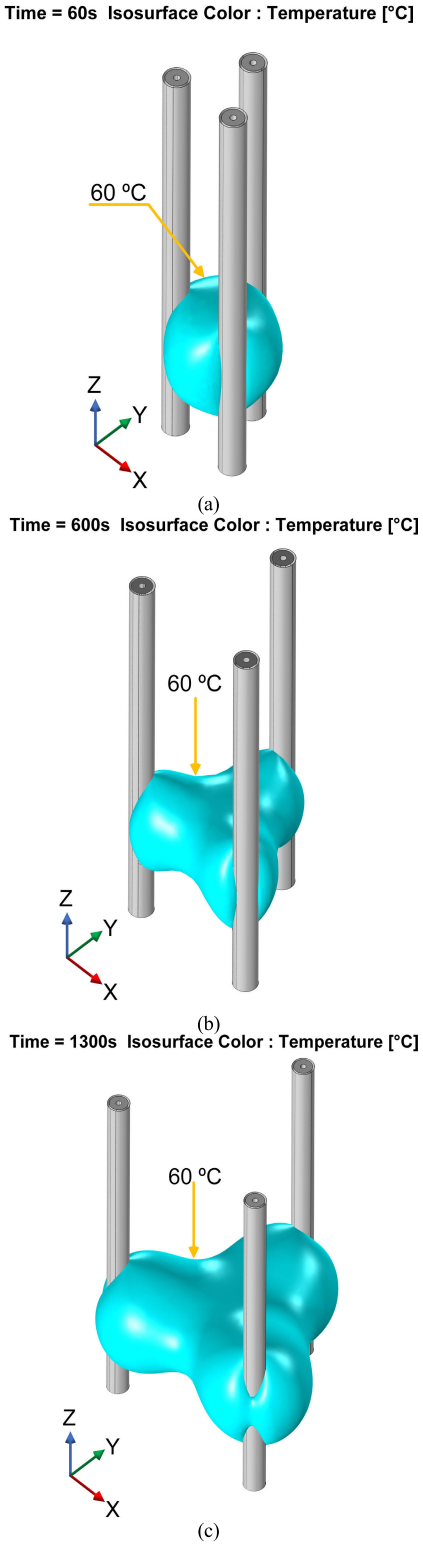

FIGURE 13. 3D FE-simulated coagulation volume using the triple-CHSA scheme, given 50 W microwave energy, for the distance between antennas of: (a) 10 mm, (b) 20 mm, (c) 30 mm.

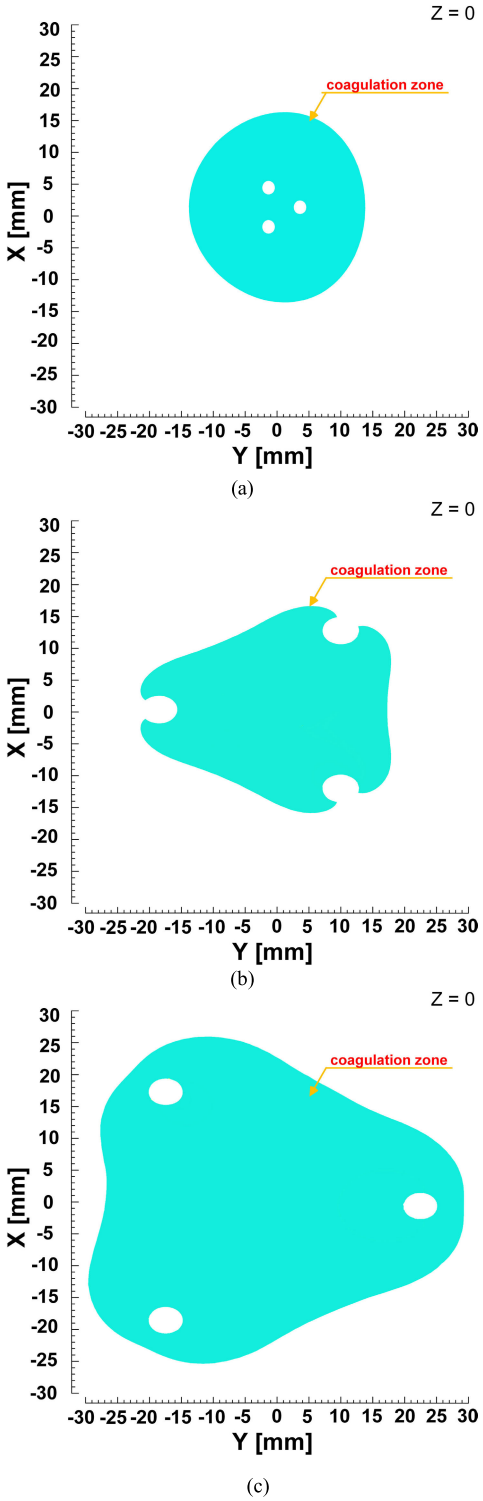

FIGURE 14. FE-simulated coagulation zone using the triple-CHSA scheme in x-y plane, given 50 W microwave energy and z = 0, for the between-antenna distances of (MW duration): (a) 10 mm (660 seconds), (b) 20 mm (1250 seconds), (c) 30 mm (2000 seconds).

IV. IN VITRO EXPERIMENTAL SETUP

Fig 6(a) and (b) are illustrates the schematic and case of in vitro experimental setup for hepatic MWA using a three-output MW source capable of controlling the MW energy levels of CHS antennas independently [8]. The MW source was a magnetron oscillator operating at 2450 MHz with maximum continuous-wave output of 250 W.

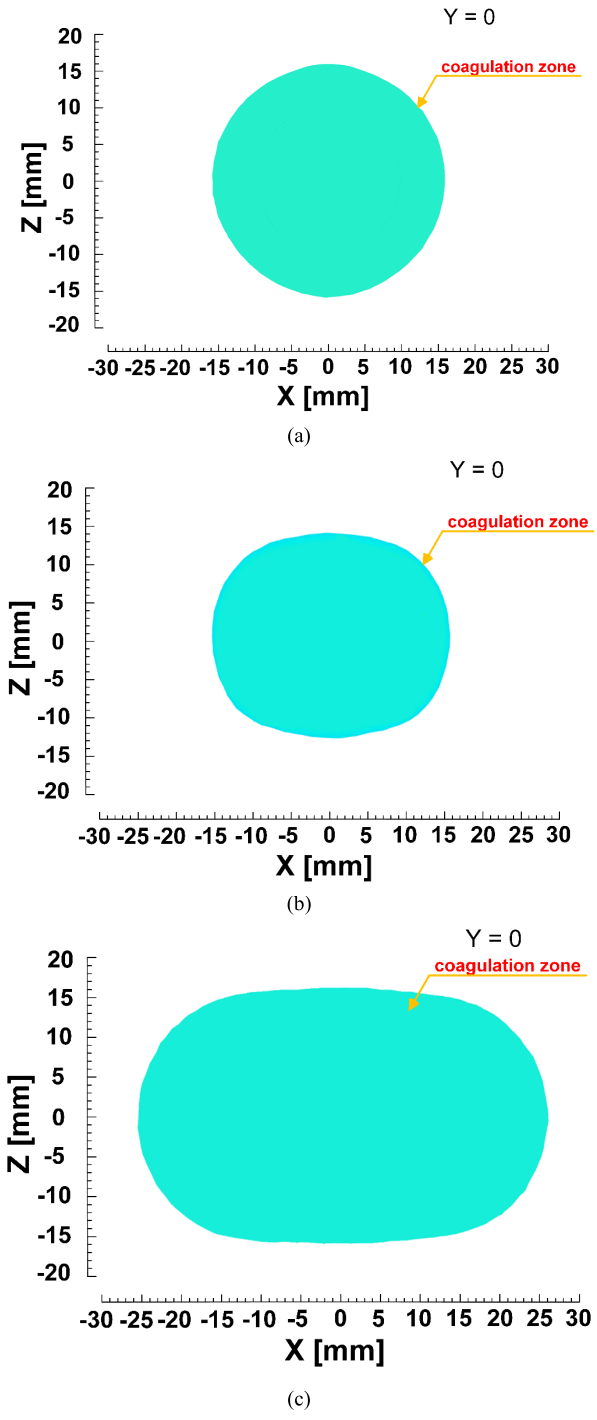

FIGURE 15. FE-simulated coagulation zone using the triple-CHSA scheme in z-x plane, given 50 W microwave energy and y = 0, for the between-antenna distances of (MW duration): (a) 10 mm (660 seconds), (b) 20 mm (1250 seconds), (c) 30 mm (2000 seconds).

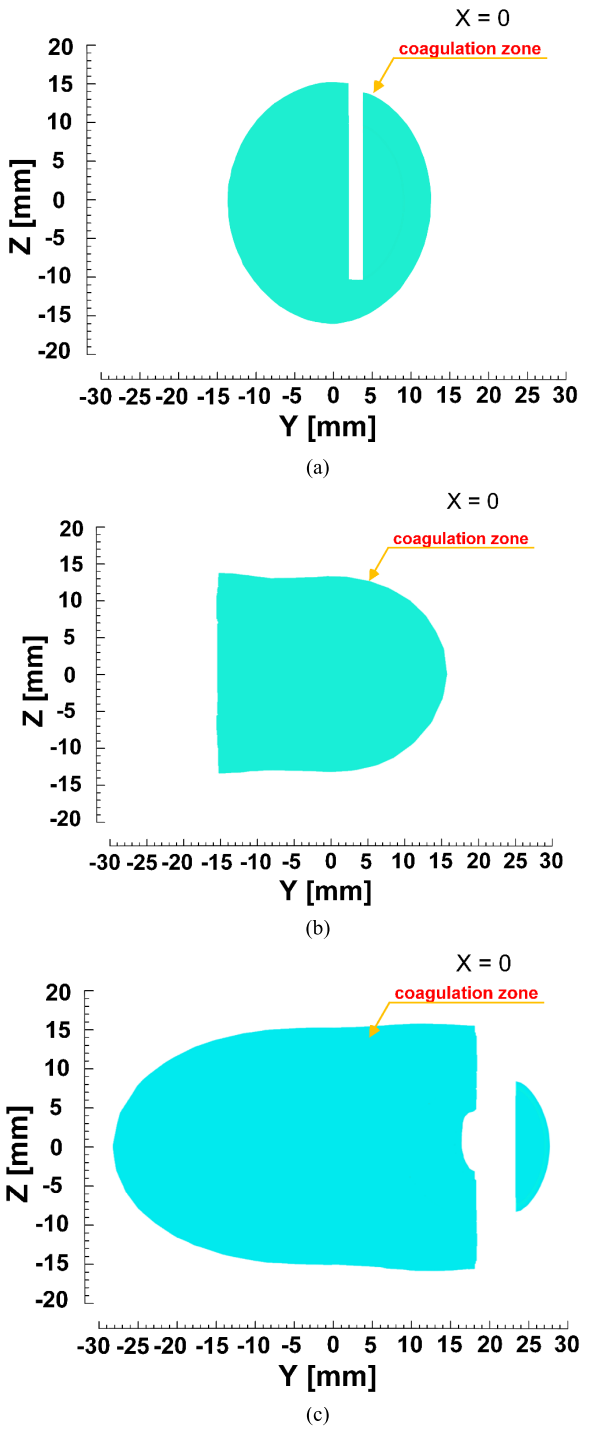

FIGURE 16. FE-simulated coagulation zone using the triple-CHSA scheme in z-y plane, given 50 W microwave energy and x = 0, for the between-antenna distances of (MW duration): (a) 10 mm (660 seconds), (b) 20 mm (1250 seconds), (c) 30 mm (2000 seconds).

The experimental setup consisted of three microwave power meters (Wideband Power Sensor Model 5012 (350 – 4000 MHz), Bird Electronic Corporation). The microwave power meters were connected to a laptop computer (Inter®Core i7-4720HQ 2.8 GHz, Windows 10 Pro, 8 GB RAM, 1 TB hard disk) via universal serial bus (USB) 2.0 cables. The triple antennas (Antennas I, II, III) were simultaneously fed with 50W microwave energy. The in vitro experimental setup also included two temperature probes. The first temperature probe (with S_c) was located at the midpoint of the triple CHSA arrangement, and the second temperature probe (with S1, S2, S3) was located 5 mm from the midpoint between Antennas I and II.

In in vitro experiment, the single CHS antenna was first experimented in egg white and swine liver using 50 W microwave energy for 100 seconds, as shown in Figs 7 (a)-(b), respectively. The egg white and swine liver were retained on a heat bed at 37 °C ([8], [28]). The single-antenna in vitro experiments were performed to characterize the coagulation shape (Fig 7(a) for white egg) and coagulation zone (Fig 7(b) for swine liver), given the temperature threshold of 60 °C or higher.

For the in vitro experiments using the triple-CHSA scheme, the experimental swine liver was of rectangular shape of 100 mm × 140 mm in dimension. The swine liver was retained on the heat bed at 37 °C. Similar to the FE simulation, the triple-CHSA scheme (Antennas I, II, and III) were individually fed with 50 W microwave power at 2450 MHz from 0 – 2000 seconds. The distance between Antennas I, II, and III was varied between 10, 20, and 30 mm, given the midpoint temperature of 100 °C. The in vitro experiments were carried out with 10 samples of swine liver under each distance, totaling 30 samples of swine liver.

The coagulation zone and volume in the swine liver under the triple-CHSA scheme, as indicated by discolored liver tissue, was determined by using a magnetic resonance imaging (MRI) machine (Phillips INGENIA-1.5T WA30, UK, type T2; Fig 7(c)). The MRI results were compared with the FE results of the triple-CHS antennas, given the midpoint temperature of 100 °C, with regard to the coagulation zone and volume in the xy, zx, and zy planes. The midpoint temperature of 100 °C is the level of temperature that achieved the largest coagulation zone and volume.

V. FINITE ELEMENT SIMULATION AND IN VITRO RESULTS

Fig 8 illustrates that the FE-simulated results using one single CHS antenna, given 50 W microwave energy for 100 seconds. Specifically, Figs 8(a)-(c) respectively show the specific absorption rate in the xz plane, the temperature distribution in the xz plane, and the 3D coagulation zone at 60°C or higher. Fig 9 shows the FE-simulated coagulation volume using one single CHS antenna from 0 – 100 seconds of operating time, given 50 W microwave energy. The FE-simulated coagulation volume at 100 seconds was 46.497 mm3, corresponding to that in Fig 8(c).

The FE-simulated results using the triple-antenna scheme (Antennas I, II, III), given 50 W microwave energy for 0 – 2000 seconds, indicated that the midpoint temperature of the triple-antenna scheme reached 60 °C after 60, 600, and 1300 seconds (i.e., MW durations) for the between-antenna distances of 10, 20, and 30 mm, respectively.

Panel (a) of Figs 10–13 show the FE-simulated coagulation zone using the triple-CHSA scheme, given the between-antenna distance of 10 mm and 60 seconds of MW duration. Specifically, Figs 11(a) and 12(a) respectively illustrate the FE-simulated coagulation zone in the z-x plane at $y = 5.77$ mm and -2.89 mm. Figs 13(a) and 14(a) show the FE-simulated coagulation zone in the x-y plane at $z = 0$ mm and the 3D simulated coagulation volume.

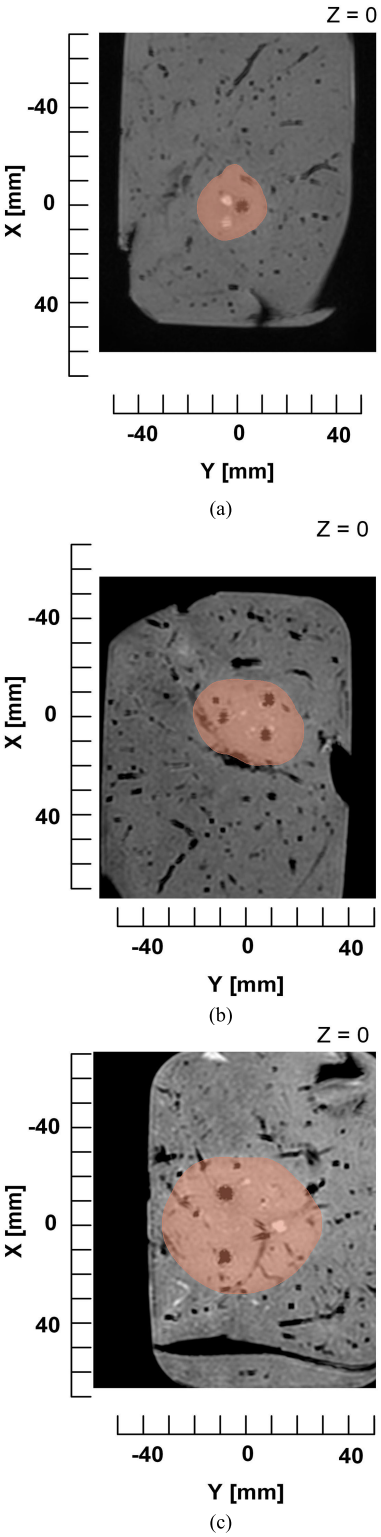

FIGURE 17. MRI images of the coagulation zone using the triple-CHSA scheme in x-y plane, given 50 W microwave energy and z = 0, for the between-antenna distances of (MW duration): (a) 10 mm (660 seconds), (b) 20 mm (1250 seconds), (c) 30 mm (2000 seconds).

Panel (b) of Figs 10–13 show the FE-simulated coagulation zone using the triple-CHSA scheme, given the between-antenna distance of 20 mm and 600 seconds of MW duration.

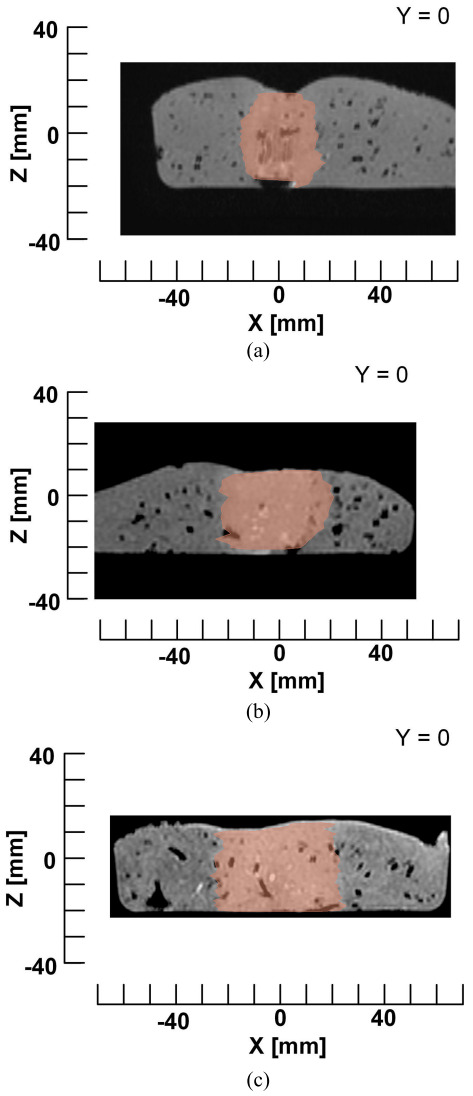

FIGURE 18. MRI images of the coagulation zone using the triple-CHSA scheme in z-x plane, given 50 W microwave energy and y = 0, for the between-antenna distances of (MW duration): (a) 10 mm (660 seconds), (b) 20 mm (1250 seconds), (c) 30 mm (2000 seconds).

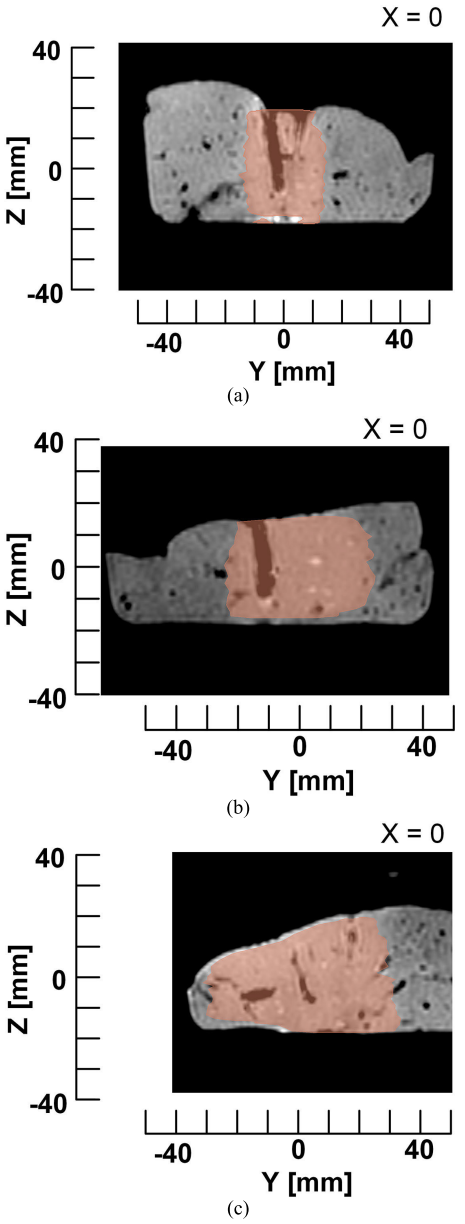

FIGURE 19. MRI images of the coagulation zone using the triple-CHSA scheme in z-y plane, given 50 W microwave energy and x = 0, for the between-antenna distances of (MW duration): (a) 10 mm (660 seconds), (b) 20 mm (1250 seconds), (c) 30 mm (2000 seconds) Note. MRI Data Highlight from specialist from hospital.

Figs 11(b) and 12(b) show the FE-simulated coagulation zone in the z-x plane at y = 11.5 mm and −5.77 mm. Figs 13(b) and 14(b) depict the FE-simulated coagulation zone in the x-y plane at z = 0 mm and the 3D simulated coagulation volume.

Panel (c) of Figs 10–13 show the FE-simulated coagulation zone using the triple-CHSA scheme, given the between-antenna distance of 30 mm and 1300 seconds of MW duration. Figs 11(c) and 12(c) show the FE-simulated coagulation zone in the z-x plane at y = 17.32 mm and −8.66 mm. Figs 13(c) and 14(c) depict the FE-simulated coagulation zone in the x-y plane at z = 0 mm and the 3D simulated coagulation volume.

Table 4 summarizes the FE-simulated coagulation zone and volume using the triple-CHSA scheme under different between-antenna distances (10, 20, 30 mm) and MW durations (60, 600, 1300 seconds), given 50 W microwave energy.

A. IN VITRO EXPERIMENTAL RESULTS

In in vitro experiments using the triple-CHSA scheme, the aim was to achieve the largest coagulation volumes in swine liver, given 50 W microwave energy. The FE-simulated results indicated that the midpoint temperature of 100 °C was achieved at 660, 1250, and 2000 seconds (MW durations) for the between-antenna distances of 10, 20, and 30 mm. As a result, the MW durations in the in vitro experiments were 660, 1250, and 2000 seconds for the corresponding between-antenna distances. The in vitro experiments were carried out with 10 samples of swine liver under each of the three between-antenna distances, resulting in 30 samples in

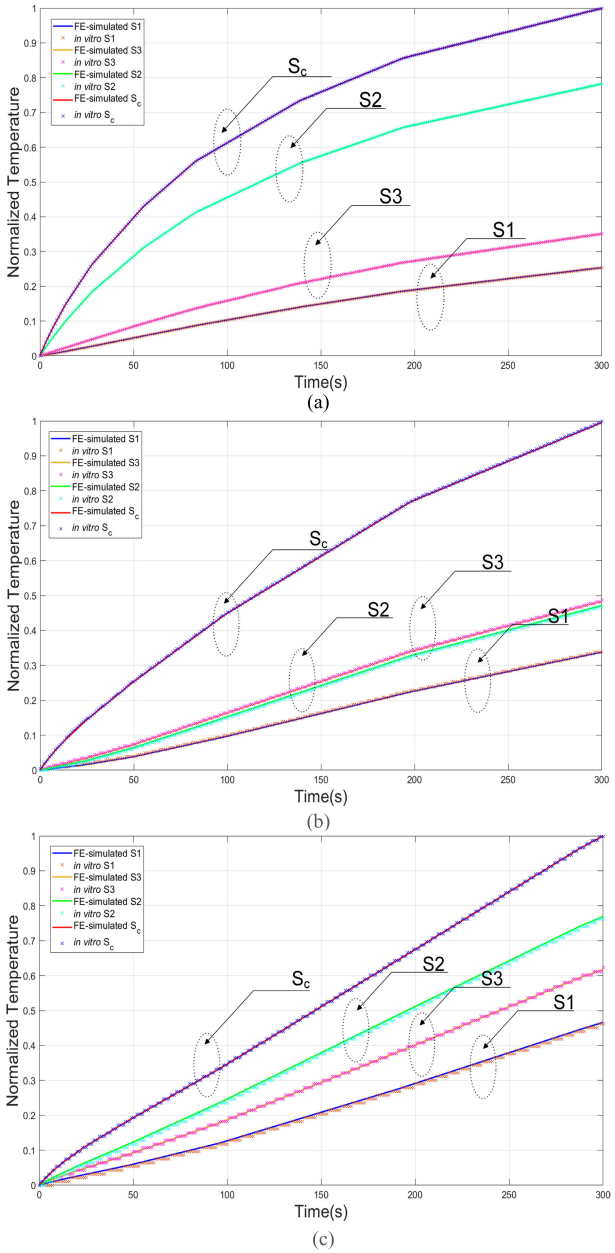

FIGURE 20. Comparison between the FE-simulated and in vitro temperature measurements for the between-antenna distance of: (a) 10 mm, (b) 20 mm, (c) 30 mm.

total. The in vitro coagulation volumes using the triple-CHSA scheme were validated against MRI images of the 30 samples of swine liver.

Panel (a) of Figs 14–16 show the FE-simulated coagulation zone using the triple-CHSA scheme in the x-y plane at z = 0; z-x plane at y = 0; and z-y plane z = 0, respectively, given the between-antenna distance of 10 mm and 660 seconds of MW duration.

Panel (b) of Figs 14–16 illustrate the FE-simulated coagulation zone using the triple-CHSA scheme in the x-y plane at z = 0; z-x plane at y = 0; and z-y plane z = 0, respectively, given the between-antenna distance of 20 mm and 1250 seconds of MW duration.

TABLE 5. FE-simulated and in vitro coagulation zone and volume using the triple-CHSA scheme.

Distance (mm)	Plane	FE simulation Width (mm)	FE simulation Length (mm)	FE simulation Volume (cm^3)	*In vitro* (MRI results) Width (mm)	*In vitro* (MRI results) Length (mm)	*In vitro* (MRI results) Volume (cm^3)
10	XY	31.2	27.1	18.425	29.8±0.5	27.0±0.7	18.437
	ZX	33.2	31.2		33.3±0.4	30.0±0.6	
	ZY	33.2	27.1		32.4±0.6	26.9±0.8	
20	XY	32.0	38.4	29.312	31.4±0.4	39.2±0.6	29.317
	ZX	27.4	32.0		28.1±0.2	33.0±0.4	
	ZY	27.4	38.5		28.2±0.5	39.3±0.4	
30	XY	52.2	57.8	63.507	51.4±0.8	58.1±0.9	63.504
	ZX	32.4	52.0		33.6±0.7	51.2±0.8	
	ZY	32.4	57.8		33.4±0.6	57.6±0.7	

Panel (c) of Figs 14–16 depict the FE-simulated coagulation zone using the triple-CHSA scheme in the x-y plane at z = 0; z-x plane at y = 0; and z-y plane z = 0, respectively, given the between-antenna distance of 30 mm and 2000 seconds of MW duration.

Figs 17(a)-(c) show the MRI images of coagulation zones using the triple-CHSA scheme in the x-y plane, given 50 W microwave energy and z = 0, for the between-antenna distances of 10, 20, and 30 mm, corresponding to Figs 14(a)-(c). Figs 18(a)-(c) illustrate the MRI images in the z-x plane and y = 0, corresponding to Figs 15(a)-(c). Meanwhile, Figs 19(a)-(c) show the MRI images in the z-y and x = 0, corresponding to Figs 16(a)-(c). The MRI results were interpreted by a specialist, and the coagulation zones were indicated by the beige color.

Table 5 compares the FE-simulated and in vitro coagulation zone and volume using the triple-CHSA scheme under three different between-antenna distances. The simulation and in vitro (MRI images) results were in good agreement.

To validate the FE model, Figs 20(a)-(c) compare the FE-simulated temperatures at the four temperature sensors (Sc, S1, S2, S3) with those of in vitro experiments using swine liver for different between-antenna distances (10, 20, and 30 mm), respectively. The simulated and experimental results were in good agreement.

VI. DEEP LEARNING ALGORITHM AND TEMPERATURE PREDICTION PERFORMANCE

The optimized weight (W) and bias (B) of the regression-based deep learning algorithm to predict the temperature of liver tissue at the midpoint of the triple-CHSA arrangement, given the between-antenna distance of 10 mm, as an example, are as follows:

Note: In the execution of the deep learning algorithm, the bias coefficients (*B1* – *B4*) were combined with the weighted features using array broadcasting (8).

$$W_1 = [0.02960265, 0.93050784, 0.55238633, 0.99678821, 0.15065016],$$
$$[-1.45968458, -1.11197986, -0.15204866, -2.34185234, 0.05243656],$$
$$[-0.18836552, -0.94471137, 0.02743533, -1.85007523, -1.25096195]$$

$$B_1 = [-0.78071878, 1.37086977, 0.53442212, -0.3064704, 0.69933807]$$

$$W_2 = [0.82911184, -0.40085982, -0.20298985, -1.83470231], [2.3693101, 1.65725503, 0.51393974, 1.59301958], [0.19485634, 0.57447295, -0.02095393, 1.62864584], [1.50224015, 0.20928054, -0.71311275, 0.09114521], [0.89329318, 1.27242794, -0.31838459, -0.11052131]$$

$$B_2 = [0.98888946, -0.34309738, -0.75127424, 0.65843885]$$

$$W_3 = [-1.33590507, -0.06509381, -0.50877751], [-0.71605194, -0.69485725, 0.20764489], [1.02513211, 0.16683648, -0.45192362], [1.42519558, 1.17132763, 0.52837088]$$

$$B_3 = [0.96577575, -1.77741594, 0.44092718]$$

$$W_4 = [0.69838018], [0.56482379], [1.02109317]$$

$$B_4 = [-0.2440661]$$

Fig 21 compares, as an example, the deep learning-based predicted normalized midpoint temperatures (Y_predict) against the in vitro temperature measurements (i.e., normalized testing output dataset (Y_test)), given the between-antenna distance of 10 mm.

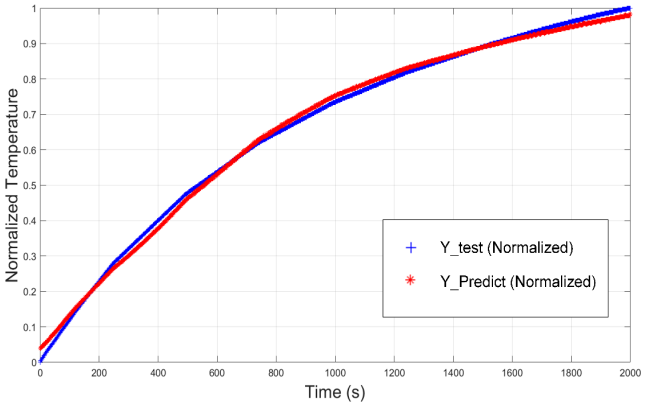

FIGURE 21. Comparison between in vitro midpoint temperature measurements (i.e., normalized testing output dataset (Y_test)) and deep learning-based predicted normalized midpoint temperatures (Y_predict), given the between-antenna distance of 10 mm.

Fig 22 illustrates the scatter plot of normalized midpoint temperatures (Y_test) relative to deep learning-based predicted normalized midpoint temperatures (Y_predict), given the between-antenna distance of 10 mm, as an example. The correlation between the normalized midpoint temperatures and deep learning-based predicted normalized midpoint temperatures was near-linear. The prediction performance

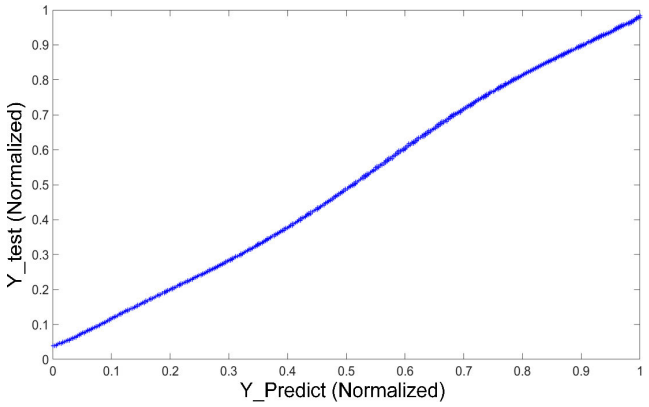

FIGURE 22. The scatter plot of normalized midpoint temperatures (Y_test) relative to deep learning-based predicted normalized midpoint temperatures (Y_predict), given the between-antenna distance of 10 mm.

TABLE 6. Comparison of Multi antenna microwave ablation.

	Research Topic	Type of antenna	Spec	Temperature sensor	Dimension of ablation size
Ref. [19]	In ex vivo, bovine liver	Single 13-gauge antenna two 17-gauge antennas three 18-gauge antennas	2.45 GHz 90W	Yes	Cross-sectional area = 25.5 mm^2
Ref. [21]	Numerical analysis effect of phase different antenna	Slot antenna Array 2 probes and 3 probes	2.45 GHz 50W	No	2 probes (180° phase shift) = 35.17 cm^3 3 probes (180° phase shift) = 49.65 cm^3
Ref. [22]	Experimental In vivo porcine liver	13-gauge dipole antenna	915 MHz 60W	Yes	Maximum lesion volume = 43.1 cm^3
Ref. [28]	3D Finite Element with In vitro experiment study effect of configuration replacement - Array - Triangle - Orthogonal	-Coaxial Slot -Open tip -Coaxial Slot with Insulator	2.45 GHz 50W	No	Maximum lesion volume = 30.7 cm^3
Purposed	3D Finite Element with In Vitro experiment with Deep learning prediction and MRI results	Directional antenna (Coaxial half slot antenna)	2.45 GHz 50W	Yes -With deep learning algorithm and without insert sensor in cancer tissue	Maximum lesion volume = 63.5 cm^3 Deep learning prediction accuracy 99.98%(MSE)

(accuracy) of the proposed deep learning algorithm to predict the temperature of liver tissue at the midpoint of the triple-CHSA scheme was 99.98 % for MSE, 98.75 % for MAE, and 99.22 % for MAPE. The higher MSE (99.98 %), vis-à-vis MAE (98.75 %), indicated that the

deep learning-based predicted midpoint temperatures closely resembled the in vitro midpoint temperature measurements. The finding validates the applicability of the proposed deep learning algorithm to predict the midpoint temperature without the need to insert the temperature sensor into the targeted liver tissue, thereby minimizing injuries to the cancer tissue.

Table 6 comparison table multi-antenna technique in Microwave Ablation shows that some systems do not use Temperature sensors. In systems where temperature sensors are used, they must be placed in the position to be measured. In actual use, it may block the transmission of electromagnetic waves in the tissues due to the placement of the antenna in cancer tissue. In this research, the researchers have used a temperature sensor placed beside the cancer tissue, which does not block the wave propagation by using deep learning to calculate the temperature in the half-distance of the cancer tissue. The result produces more significant amounts of cancer tissue destruction than previous studies.

VII. CONCLUSION

This research proposed a triple-antenna scheme for minimally invasive hepatic MWA. The triple-antenna scheme consisted of three CHSA surrounding the cancer tissue in equilateral triangle formation, with the half-slot side of the three antennas directed at the midpoint of the triangle to concentrate the microwave energy at the center. The distance between the three antennas was varied between 10, 20, and 30 mm. FE simulations and in vitro experiments with swine liver were carried out to determine the temperatures and coagulation zone under three between-antenna distances. The triple-CHSA scheme could achieve a large coagulation zone with temperatures of 60 °C or higher. Moreover, a regression-based deep learning algorithm was proposed to predict temperatures of the liver tissue at the midpoint of the triple-CHSA arrangement without the need to insert a temperature sensor into the targeted cancer tissue. The algorithm relied on temperatures at the site adjacent to the targeted cancer tissue to predict the midpoint temperature.

The FE simulation results showed that the triple-CHSA scheme could achieve the largest coagulation volumes of 18.425, 29.312, and 63.507 cm^3 for the between-antenna distances of 10, 20, and 30 mm, respectively. The largest coagulation volumes of in vitro experiments based on MRI images were 18.437, 29.317, and 63.504 cm^3 for the corresponding between-antenna distances. Furthermore, the prediction accuracy of the proposed deep learning algorithm to predict the midpoint temperature were 99.98 % for MSE, 98.75 % for MAE, and 99.22 % for MAPE. The performance validates the applicability of the deep learning algorithm to predict the midpoint temperature without the need to insert a temperature sensor into the targeted liver tissue.

The novelty of the research lies in the use of CHSA surrounding the cancer tissue in equilateral triangle formation for hepatic MWA, as opposed to the conventional hepatic MWA procedure which requires inserting antennas into the targeted tissue. Another research novelty is the use of regression-based deep learning algorithm to predict the temperature of liver tissue at the midpoint of the triple-CHSA arrangement.

ACKNOWLEDGMENT

The authors would like to express deep gratitude to Siriraj Hospital Thailand for support MRI and expert for checked and Validated data.

REFERENCES

[1] V. Mohan. (2019). *Liver Cancer (Hepatocellular Carcinoma)*. [Online]. Available: https://www.medicinenet.com/liver_cancer_hepatocellular_carcinoma/article.htm

[2] S. N. Goldberg, G. S. Gazelle, L. Solbiati, T. Livraghi, K. K. Tanabe, P. F. Hahn, and P. R. Mueller, "Ablation of liver tumors using percutaneous RF therapy," *AJR. Amer. J. Roentgenol.*, vol. 170, no. 4, pp. 1023–1028, 1998.

[3] R. Lencioni, O. Goletti, N. Armillotta, A. Paolicchi, M. Moretti, D. Cioni, F. Donati, A. Cicorelli, S. Ricci, M. Carrai, P. F. Conte, E. Cavina, and C. Bartolozzi, "Radio-frequency thermal ablation of liver metastases with a cooled-tip electrode needle: Results of a pilot clinical trial," *Eur. Radiol.*, vol. 8, no. 7, pp. 1205–1211, Sep. 1998.

[4] G. Todorov, C. Bachvarov, G. Valchev, N. Kolev, A. Tonev, V. Ignatov, K. Ivanov, E. Dimitrova, N. Conev, and S. Sirakov, "Radiofrequency ablation of unresectable primary and metastatic hepatic malignancies," *Varna Med. Forum*, vol. 7, no. 1, pp. 11–14, 2018.

[5] J. Seifert, T. Junginger, and D. Morris, "A collective review of the world literature on hepatic cryotherapy," *J. Roy. College Surgeons Edinburgh*, vol. 43, no. 3, pp. 141–154, 1998.

[6] S. Curto, M. Taj-Eldin, D. Fairchild, and P. Prakash, "Microwave ablation at 915 MHz vs 2.45 GHz: A theoretical and experimental investigation," *Med. Phys.*, vol. 42, no. 11, pp. 6152–6161, Nov. 2015.

[7] F.-Y. Liu, X.-L. Yu, P. Liang, Y. Wang, P. Zhou, and J. Yu, "Comparison of percutaneous 915 MHz microwave ablation and 2450 MHz microwave ablation in large hepatocellular carcinoma," *Int. J. Hyperthermia*, vol. 26, no. 5, pp. 448–455, Aug. 2010.

[8] K. Ito, H. Yoshimura, Y. Hayashi, and K. Saito, "Heating characteristics of array applicator composed of two coaxial-slot antennas for microwave coagulation therapy," *IEEE Trans. Microw. Theory Techn.*, vol. 48, no. 11, pp. 1800–1806, Nov. 2000.

[9] S. A. Shock, K. Meredith, T. F. Warner, L. A. Sampson, A. S. Wright, T. C. Winter, D. M. Mahvi, J. P. Fine, and F. T. Lee, "Microwave ablation with loop antenna: *In vivo* porcine liver model," *Radiology*, vol. 231, no. 1, pp. 143–149, Apr. 2004.

[10] C. L. Brace, P. F. Laeseke, D. W. van der Weide, and F. T. Lee, "Microwave ablation with a triaxial antenna: Results in *ex vivo* bovine liver," *IEEE Trans. Microw. Theory Techn.*, vol. 53, no. 1, pp. 215–220, Jan. 2005.

[11] P. Punit, M. C. Converse, J. G. Webster, and D. M. Mahvi, "An optimal sliding choke antenna for hepatic microwave ablation," *IEEE Trans. Biomed. Eng.*, vol. 56, no. 10, pp. 2470–2476, Oct. 2009.

[12] C. J. T. Romero, G. R. Martinez, L. L. Salas, A. V. Hernandez, and J. G. Martinez, "Micro-coaxial slot antenna to treat bone tumors by thermal ablation: Theoretical and experimental evaluation," *IEEE Latin Amer. Trans.*, vol. 16, no. 11, pp. 2731–2737, Nov. 2018.

[13] J. C. Lin and Y.-J. Wang, "The cap-choke catheter antenna for microwave ablation treatment," *IEEE Trans. Biomed. Eng.*, vol. 43, no. 6, pp. 657–660, Jun. 1996.

[14] D. Yang, J. M. Bertram, M. C. Converse, A. P. O'Rourke, J. G. Webster, S. C. Hagness, J. A. Will, and D. M. Mahvi, "A floating sleeve antenna yields localized hepatic microwave ablation," *IEEE Trans. Biomed. Eng.*, vol. 53, no. 3, pp. 533–537, Mar. 2006.

[15] C. L. Brace, "Dual-slot antennas for microwave tissue heating: Parametric design analysis and experimental validation," *Med. Phys.*, vol. 38, no. 7, pp. 4232–4240, Jun. 2011.

[16] M. Ge, H. Jiang, X. Huang, Y. Zhou, D. Zhi, G. Zhao, Y. Chen, L. Wang, and B. Qiu, "A multi-slot coaxial microwave antenna for liver tumor ablation," *Phys. Med. Biol.*, vol. 63, no. 17, Sep. 2018, Art. no. 175011.
[17] P. Nantivatana, P. Phasukkit, S. Tungjitkusolmun, and K. Chayakulkheeree, "Optimal antenna slot design for hepatocellular carcinoma microwave ablation using multi-objective fuzzy decision making," *Int. J. Intell. Eng. Syst.*, vol. 13, no. 5, pp. 38–50, Oct. 2020.
[18] W. Wongtrairat, P. Phasukkit, S. Tungjitkusolmun, and P. Nantivatana, "The effect of slot sizes on non-asymmetry slot antennafor microwave coagulation therapy," *Int. J. Biosci., Biochem. Bioinf.*, vol. 1, no. 3, pp. 192–198, 2011.
[19] P. F. Laeseke, F. T. Lee, Jr., D. W. van der Weide, and C. L. Brace, "Multiple-antenna microwave ablation: Spatially distributing power improves thermal profiles and reduces invasiveness," *J. Intervent. Oncol.*, vol. 2, no. 2, p. 65, 2009.
[20] M. Selmi, A. A. B. Dukhyil, and H. Belmabrouk, "Numerical analysis of human cancer therapy using microwave ablation," *Appl. Sci.*, vol. 10, no. 1, p. 211, Dec. 2019.
[21] P. Phasukkit, S. Tungjitkusolmun, and A. Sanpanich, "Finite element analysis on phase shift effect of multi-antenna array alignment for microwave liver ablation," in *Proc. IEEE-EMBS Conf. Biomed. Eng. Sci.*, Dec. 2012, pp. 326–329.
[22] A. S. Wright, F. T. Lee, and D. M. Mahvi, "Hepatic microwave ablation with multiple antennae results in synergistically larger zones of coagulation necrosis," *Ann. Surgical Oncol.*, vol. 10, no. 3, pp. 275–283, Apr. 2003.
[23] A. Karampatzakis, S. Kühn, G. Tsanidis, E. Neufeld, T. Samaras, and N. Kuster, "Heating characteristics of antenna arrays used in microwave ablation: A theoretical parametric study," *Comput. Biol. Med.*, vol. 43, no. 10, pp. 1321–1327, Oct. 2013.
[24] K. Saito, T. Taniguchi, H. Yoshimura, and K. Ito, "Estimation of SAR distribution of a tip-split array applicator for microwave coagulation therapy using the finite element method," *IEICE Trans. Electron.*, vol. E84-C, no. 7, pp. 948–954, 2001.
[25] A. S. Wright, D. M. Mahvi, D. G. Haemmerich, and F. T. Lee, Jr., "Minimally invasive approaches in management of hepatic tumors," *Surgical Technol. Int.*, vol. 11, pp. 144–153, Jan. 2003.
[26] B. T. McWilliams, E. E. Schnell, S. Curto, T. M. Fahrbach, and P. Prakash, "A directional interstitial antenna for microwave tissue ablation: Theoretical and experimental investigation," *IEEE Trans. Biomed. Eng.*, vol. 62, no. 9, pp. 2144–2150, Sep. 2015.
[27] P. Liang, B. Dong, X. Yu, D. Yu, Z. Cheng, L. Su, J. Peng, Q. Nan, and H. Wang, "Computer-aided dynamic simulation of microwave-induced thermal distribution in coagulation of liver cancer," *IEEE Trans. Biomed. Eng.*, vol. 48, no. 7, pp. 821–829, Jul. 2001.
[28] P. Phasukkit, S. Tungjitkusolmun, and M. Sangworasil, "Finite-element analysis and *in vitro* experiments of placement configurations using triple antennas in microwave hepatic ablation," *IEEE Trans. Biomed. Eng.*, vol. 56, no. 11, pp. 2564–2572, Nov. 2009.

PATTARAPONG PHASUKKIT (Member, IEEE) was born in Saraburi, Thailand, in May 1978. He received the B.Eng. and M.Eng. degrees in telecommunications and the D.Eng. degree in electrical engineering from the Department of Electronics, School of Engineering, King Mongkut's Institute of Technology Ladkrabang (KMITL), Bangkok, Thailand, in 2000, 2003, and 2009, respectively, where he is currently working as an Associate Professor. His current research interests include microwave ablation, antenna design, and wireless communications.

TEERASAK WONGKETSADA was born in Trang, Thailand, in March 1997. He received the B.Eng. degree in biomedical engineering from the Department of Electronics, King Mongkut's Institute of Technology Ladkrabang (KMITL), Bangkok, Thailand, in 2019, where he is currently pursuing the master's degree in electronic engineering. His current research interests include microwave ablation, antenna design, and biomedical engineering.